Available online at www.sciencedirect.com

ScienceDirect

Geochimica et Cosmochimica Acta 197 (2017) 215–225

Geochimica et Cosmochimica Acta

www.elsevier.com/locate/gca

Efficacy of ^{230}Th normalization in sediments from the Juan de Fuca Ridge, northeast Pacific Ocean

Kassandra Costa *, Jerry McManus

Lamont-Doherty Earth Observatory of Columbia University, Palisades, NY 10964, USA
Department of Earth and Environmental Sciences, Columbia University, New York, NY 10027, USA

Received 2 June 2016; accepted in revised form 22 October 2016; Available online 29 October 2016

Abstract

^{230}Th normalization is an indispensable method for reconstructing sedimentation rates and mass fluxes over time, but the validity of this approach has generated considerable debate in the paleoceanographic community. ^{230}Th systematics have been challenged with regards to grain size bias, sediment composition ($CaCO_3$), water column advection, and other processes. In this study, we investigate the consequences of these effects on ^{230}Th normalization from a suite of six cores on the Juan de Fuca Ridge. The proximity of these cores (<30 km) suggests that they should receive the same particle rain rate of sediment, but the steep bathymetry of the ridge leads to substantial sediment redistribution and variable carbonate preservation, both of which may limit the usage of ^{230}Th in this region. Despite anticipated complications, ^{230}Th normalization effectively reconstructs nearly identical particle rain rates from all six cores, which are summarily unrelated to the total sedimentation rates as calculated from the age models. Instead the total sedimentation rates are controlled almost entirely by sediment focusing and winnowing, which are highly variable even over the short spatial scales investigated in this study. Furthermore, no feedbacks on ^{230}Th systematics were detected as a consequence of sediment focusing, coarse fraction variability, or calcium carbonate content, supporting the robustness of the ^{230}Th normalization technique.
© 2016 Elsevier Ltd. All rights reserved.

Keywords: ^{230}Th normalization; Sediment focusing; Juan de Fuca Ridge

1. INTRODUCTION

Particle rain rate is one of the vital signs of the surface ocean. Changes in the abundance and composition of surface particles are fundamental to reconstructing productivity and carbon export over time. Gravimetric analyses of biological sedimentary components (opal, carbonate, organic carbon) integrate the production at the surface with dilution and preservation effects at the seafloor, and only by knowing the total particle rain rate can the mass fractions translate into absolute fluxes. Traditionally, particle rain rates are calculated using the age model tie points and the intervening sediment thickness to determine the average sedimentation rate over that time period (e.g., Broecker, 1971). But this method is confounded by the omnipresent sediment redistribution on the seafloor (Johnson and Johnson, 1970; Bacon, 1984; Francois et al., 2004), which appends a horizontal sediment flux onto the vertical particle rain. Age model based sedimentation rates can only reconstruct the total sediment delivery (vertical + horizontal), and significant sediment focusing in, e.g., drift deposits can lead to astonishingly high total sedimentation rates of 100 cm/kyr or more (e.g., Keigwin and Schlegel, 2002). Using these age model-based total sedimentation rates as a stand-in for particle rain rates can lead to severe misinterpretations of the climatic and oceanographic history of a region (as discussed in Francois et al., 2004; Kienast

* Corresponding author.
E-mail addresses: kcosta@ldeo.columbia.edu (K. Costa), jmcmanus@ldeo.columbia.edu (J. McManus).

http://dx.doi.org/10.1016/j.gca.2016.10.034
0016-7037/© 2016 Elsevier Ltd. All rights reserved.

et al., 2007). The need for reliable proxies for the particle rain rate has led to the development of age-model independent techniques using constant flux proxies, like ^{230}Th.

Constant flux proxies (^{230}Th, ^{3}He) have well-constrained source functions, and the flux of these nuclides to the sediment is known and constant. Therefore, their concentration in the sediment depends on the same dilution effects that influence surface productivity indicators like opal and organic carbon. These dilution effects are driven by changes in the particle rain rate, and normalizing to a constant flux proxy, especially ^{230}Th, has several clear advantages over the age model based reconstructions of sedimentation (Bacon, 1984; Suman and Bacon, 1989; Francois et al., 1990, 2004). First, ^{230}Th normalization allows point-by-point calculation of sedimentation rate regardless of and generally at much higher resolution than age model tie-points. Second, ^{230}Th can distinguish between vertical and lateral sediment contributions because sediment focusing or winnowing would result in excess or deficient ^{230}Th compared to the known production rate. Finally since ^{230}Th specifically reconstructs particle rain rates, ^{230}Th-based sedimentation rates are more regionally homogeneous (Ruhlemann et al., 1996; Kienast et al., 2007; Anderson et al., 2008) than age model based sedimentation rates, which can show wide variations on scales as small as kilometers (Johnson and Johnson, 1970; Costa et al., 2016).

No proxy is perfect, and several shortcomings of the ^{230}Th technique have also been identified. Despite its short residence time in the water column (20–40 years) some diffusion and advection of ^{230}Th along concentration gradients leads to boundary scavenging and ^{230}Th fluxes elevated above the constant production rate (Anderson et al., 1983; Henderson et al., 1999; Lyle et al., 2005; Broecker, 2008; Singh et al., 2013). Similarly, ^{230}Th surpluses could occur as a result of preferential remobilization of fine sediments, which contain the majority of adsorbed ^{230}Th due to their high surface area (Suman and Bacon, 1989; Kretschmer et al., 2010; Lyle et al., 2014). Both water column transport and sediment focusing could decouple ^{230}Th from the particle rain rate, dissolving the foundation from which ^{230}Th is used as a constant flux proxy. The magnitude of these effects and the implications for ^{230}Th normalization have led to considerable debate about its application for reconstructing sediment fluxes, particularly in carbonate rich sediments in the Equatorial Pacific (Lyle et al., 2005, 2007, 2014; Francois et al., 2007; Broecker, 2008; Marcantonio et al., 2014). Whether or not these challenges are regionally specific to the Equatorial Pacific or evident of a broader global pattern has yet to be established.

This paper investigates the utility of ^{230}Th normalization in sediments on the Juan de Fuca Ridge (JdFR), where rough topography generates substantial sediment focusing and winnowing (Costa et al., 2016). Age model based sedimentation rates range over an order of magnitude despite the expectation that the tightly gridded suite of cores (6 cores within 50 km) should receive nearly identical surface particle rain rates. Comparing the ^{230}Th-based sedimentation rates from these cores over the past 400–500,000 years will ascertain if the degree of sediment redistribution affects the ability of ^{230}Th to reconstruct particle rain rates. If sediment focusing has little to no effect on ^{230}Th systematics, then all six cores should yield the same ^{230}Th based sedimentation rate. If sediment redistribution decouples ^{230}Th from the particle rain rate, then the six cores will likely produce different ^{230}Th based sedimentation rates, which may instead scale with age model based total sedimentation rates, the fraction of fine sediment, or the carbonate content.

2. MATERIALS & METHODS

2.1. Core sites and stratigraphy

Samples were taken from six cores on the Juan de Fuca Ridge (Fig. 1) collected on the SeaVOICE cruise (AT26-19) of the R/V Atlantis in September 2014. Cores were retrieved in two E-W transects in a semi-grid on the western flanks of the ridge, targeted on ridge-parallel crests (2655–2794 m) to maximize carbonate preservation (Costa et al., 2016). The average spacing between cores is about 20 km. Utilizing a tight cluster of cores underlying one productivity regime eliminates the variability associated with crossing surface productivity gradients, which have characterized previous studies employing meridional transects (Lyle et al., 2005; Kienast et al., 2007; Mitchell and Huthnance, 2013; Marcantonio et al., 2014).

Age models for the JdFR cores are well-constrained based on radiocarbon dates, benthic δ^{18}O, and stratigraphically-tuned density cycles (Costa et al., 2016). Both density and coarse fraction >63 μm density (Costa et al., 2016) show distinct glacial-interglacial cycles, with high-density, coarse sediment characterizing glacial deposition. Carbonate concentrations, measured by the standard coulometric method, are consistent with carbonate-rich glacial periods and carbonate-poor interglacial periods (Supplemental Fig. 1).

2.2. U-Th isotopic analyses

Samples ($n = 1097$) were analyzed for thorium (^{230}Th, ^{232}Th) and uranium (^{238}U, ^{235}U, ^{234}U) by isotope dilution inductively coupled plasma mass spectrometry (ICP-MS). In a randomized order, samples (100 mg) were spiked with ^{229}Th and ^{236}U and processed with complete acid digestion and column chromatography (Fleisher and Anderson, 2003). Isotopes were measured on an Element 2 ICP-MS at Lamont-Doherty Earth Observatory (LDEO) of Columbia University. Discrete sediment aliquots ($n = 106$) of an internal sediment standard (VOICE Internal MegaStandard, VIMS) were processed and analyzed for quality control, and these total replicates of VIMS indicate that the analytical procedure and measurement are externally reproducible within 6.2% on ^{238}U, 3.7% on ^{232}Th, and 4.9% on ^{230}Th (Fig. 2). Excess initial ^{230}Th ($^{230}Th^{0}_{xs}$, hereafter ^{230}Th) was calculated by correcting for supported decay from lithogenic and authigenic uranium (Henderson and Anderson, 2003). Lithogenic uranium concentrations were determined using a detrital ^{238}U/^{232}Th of 0.48, the value which ^{238}U/^{232}Th reaches as the ^{232}Th concentration

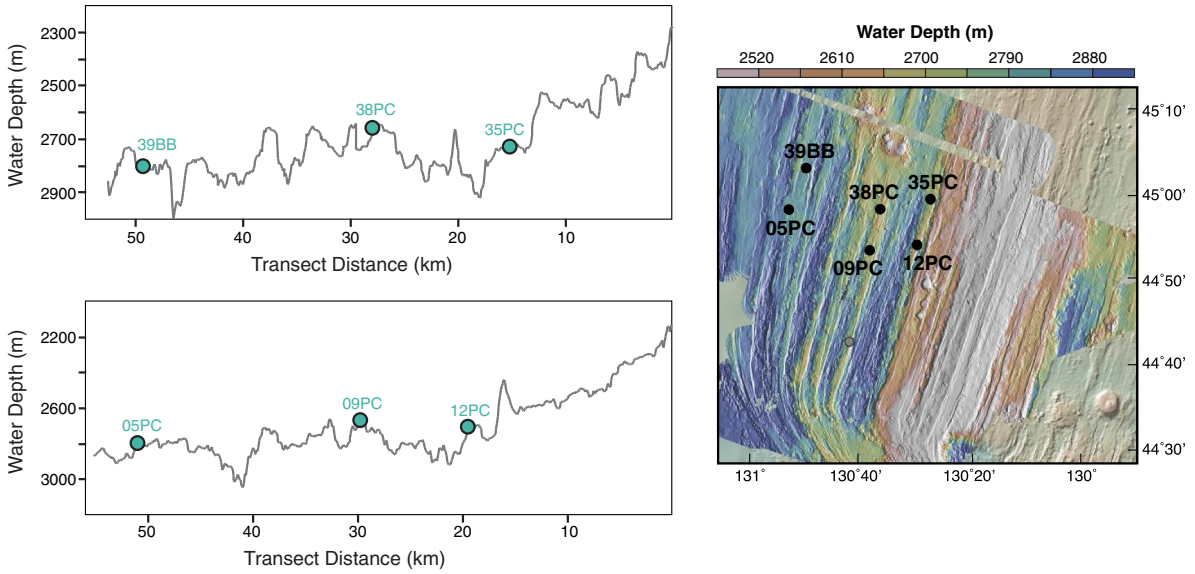

Fig. 1. Core locations on the Juan de Fuca Ridge. (*Right*) Bathymetric map by shipboard multibeam data showing the location of the Juan de Fuca cores relative to the ridge crest (in white). The cores were collected along two east–west transects. (*Left*) Bathymetric profiles from the ridge through the core locations at both the northern and southern transects. All cores were taken from relative bathymetric highs.

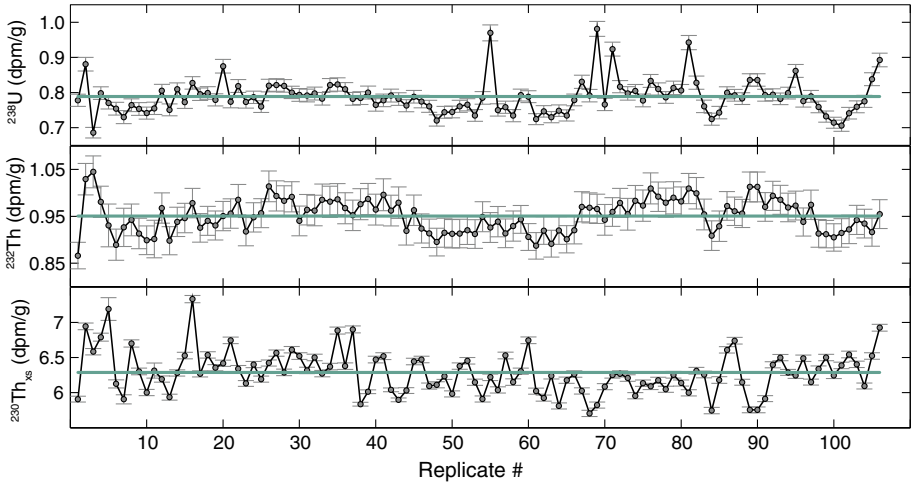

Fig. 2. VIMS replicates. The Voice Internal MegaStandard (VIMS) was analyzed repeatedly ($n = 106$) to assess reproducibility and to correct for inter-run offsets. Reproducibility is within 6% for all isotopes.

approaches its average lithogenic value (10.7 ppm, Taylor and McLennan, 1995). Corrections for supported ^{230}Th become significant as the sediment ages: supported ^{230}Th remains constant while excess ^{230}Th decays away, increasing the supported to excess ^{230}Th ratio over time. By about 400 ka, excess ^{230}Th composes less than 25% of the total ^{230}Th on the Juan de Fuca Ridge, compared to 99% excess ^{230}Th in the core tops. The loss of excess ^{230}Th substantially increases the propagated errors, reported throughout as 2σ.

2.3. ^{230}Th normalization

^{230}Th is produced in the water column by the decay of ^{234}U. Uranium is highly soluble in seawater, with a fairly constant concentration (3.2 ppb) that scales conservatively with salinity (Owens et al., 2011). The long residence time (400 kyr) of uranium leads to a relatively uniform production of ^{230}Th ($\beta_{230} = 2.555*10^{-5}$ dpm/cm^3 kyr) across the global ocean. Unlike uranium, thorium is practically insoluble in seawater, and it is quickly removed by scavenging onto settling particles and burial in the underlying sediments, so that its decay is no longer supported by its parent nuclide. The residence time of ^{230}Th in the ocean is so short (20–40 years; Nozaki et al., 1981) compared to its half-life (75,584 years; Cheng et al., 2013) that virtually all of the ^{230}Th produced by uranium decay in seawater is removed to sediments by scavenging.

The residence time of ^{230}Th is also much less than the time scale for lateral transport by mixing from regions of low scavenging intensity (low particle flux) to regions of

high scavenging intensity. Consequently, in at least 70% of the ocean the flux of ^{230}Th carried to the seafloor by sinking particles is within ~30% of its production rate in the overlying water column (Henderson et al., 1999; Henderson and Anderson, 2003). Given a rate of supply that depends mainly on water depth, the concentration of excess ^{230}Th in the underlying sediment is a function of the particle flux (PF). Higher PF will dilute the excess ^{230}Th concentration in the sediment. Thus the PF can be calculated as follows:

$$PF = \beta * z/\text{excess}^{230}\text{Th}_0$$

where β*z is the integrated ^{230}Th production (P_{Th}) in the overlying water column, and excess $^{230}Th_0$ is the concentration of excess ^{230}Th in the sediment corrected for decay since deposition (Bacon, 1984; McManus et al., 1998; Henderson and Anderson, 2003; Francois et al., 2004). Corrections for fluctuations of sea level over time are negligible and within error of the ^{230}Th measurements. From there, the sedimentation rates (cm/kyr) of particles, or particle rain rate (PRR), can be calculated by scaling the particle flux (g/cm^2 kyr) by the dry bulk density (ρ, g/cm^3):

$$PRR = PF/\rho$$

Specifically, the PRR records the sedimentation of preserved particles, and it cannot reconstruct those particles that may have suffered dissolution in the water column or on the seafloor.

2.4. Calculating focusing factors (Ψ)

The degree of sediment focusing (Ψ) can be calculated by comparing the inventory of ^{230}Th in a dated sediment horizon with the inferred production of ^{230}Th in the overlying water column over the duration of the sediment deposition (Suman and Bacon, 1989):

$$\Psi = \frac{\rho \int_{z1}^{z2} {}^{230}Th_{xs}^{0} dz}{P_{Th}(\Delta t)} \approx \frac{\rho \overline{{}^{230}Th_{xs}^{0}}(\Delta z)}{P_{Th}(\Delta t)}$$

When $\Psi = 1$, the amount of ^{230}Th buried in the sediment is equivalent to the amount produced in the water column. When $\Psi < 1$, the amount of ^{230}Th buried is less than that produced, suggesting that ^{230}Th has been removed, for example by lateral transport or winnowing of a ^{230}Th-rich sedimentary phase. Conversely, $\Psi > 1$ indicates an excess of ^{230}Th over the amount produced in the water column, primarily due to ponding of ^{230}Th-containing sediment, although it could also reflect boundary scavenging or focusing of a ^{230}Th-enriched sedimentary phase.

Focusing factors can be quite sensitive to the temporal integration periods (Kienast et al., 2007), and age model uncertainties on the order of several thousand years can propagate into substantial errors on focusing factors calculated over short periods of time (Francois et al., 1990). Previous studies have targeted deglacial time scales (5–10 kyr), but small age model adjustments can change focusing factor calculations on these timescales by as much as 100% (Loubere et al., 2004; Kienast et al., 2007). Therefore, this study only investigates full MIS focusing factors, which should be more robust against temporal uncertainties. Focusing factors were calculated by integrating ^{230}Th data from peak conditions of each MIS, covering durations ranging from 12.5–61.9 kyr and averaging 48.5 kyr. Errors were propagated using the standard deviation of the ^{230}Th within the MIS and assuming a 10% error on the age, a conservative estimate as errors >15 kyr are unlikely given the stratigraphic constraints of the age model (Costa et al., 2016).

3. RESULTS

The particle fluxes show a coherent pattern of glacial maxima and interglacial minima across all six cores (Fig. 3). Glacial periods average 0.98 g/cm^2 kyr, which is nearly double the average flux during interglacial periods (0.53 g/cm^2 kyr). The transitions between high and low flux regimes are particularly abrupt at the boundaries between glacial and interglacial periods (Termination I, ~17 ka, and Termination II, ~130 ka), while transitions associated with later glacial-interglacial boundaries are less consistent across the multiple core sites. Glacial onset tends to be gradual, with a relatively smooth increase into high glacial fluxes. In general, 12PC and 38PC tend to have the highest particle fluxes, while 05PC and 39BB have the lowest fluxes.

Because not all cores extend the full 500 kyr, we recount the trends in particle flux backwards through time, from the young coretops (6 cores) to the end of the records (2 cores). All cores contain a deglacial particle flux maximum ~20 ka that peaks at 1.5 g/cm^2 kyr and lasts about 10 kyr. Particle fluxes are fairly stable throughout MIS2-3-4 at 0.75–0.9 g/cm^2 kyr before decreasing to interglacial values (0.29–0.53 g/cm^2 kyr) at the MIS4-5 boundary. MIS5 is fairly stable, with one minor mass flux deviation (0.9 g/cm^2 kyr) occurring at 112 ka (MIS5.4-MIS5.3 transition) in 38PC. Several cores (05PC, 38PC, and 39BB) contain a deglacial particle flux maxima ~135 ka, but it is not as prominent (~1.3 g/cm^2 kyr) as the peak at Termination I. MIS6 is similar to MIS2-3-4 in terms of stability but with a slightly higher mean flux (0.88–1.33 g/cm^2 kyr), and the transition between MIS6 and MIS7 is gradual. MIS7 is similar to MIS5 in terms of both stability and amplitude (0.29–0.47 g/cm^2 kyr). MIS8 is more variable, with 12PC, 35PC, 38PC, and 39BB showing abrupt termination while 05PC and 09PC contain a gradual decrease in particle flux. Late MIS8 reaches consistent glacial particle fluxes (1.00–1.72 g/cm^2 kyr) with MIS2 and MIS6, but they are preceded by a short pulse of high particle flux (up to 13 g/cm^2 kyr) associated with the prominent magnetic susceptibility peak at 272 ka (Costa et al., 2016). Early MIS8 appears more similar to interglacial particle flux values, and the transition between MIS8-MIS9 is not readily apparent. Older glacial periods, particularly MIS10 but also MIS12, are not as homogeneous across all six cores. The particle flux maxima in MIS10 can be identified in 39BB and 12PC at glacial values (1.11–1.60 g/cm^2 kyr), but in 05PC, 09PC, and 38PC the particle flux reaches only intermediate values of 0.55–0.81 g/cm^2 kyr. MIS12 termination occurs later in 05PC than it does in 09PC, 12PC, and 38PC, potentially reflecting age model offsets. Particle fluxes during MIS12 tend to be higher (1.2–2.59 g/cm^2 kyr) than observed in later glacial periods.

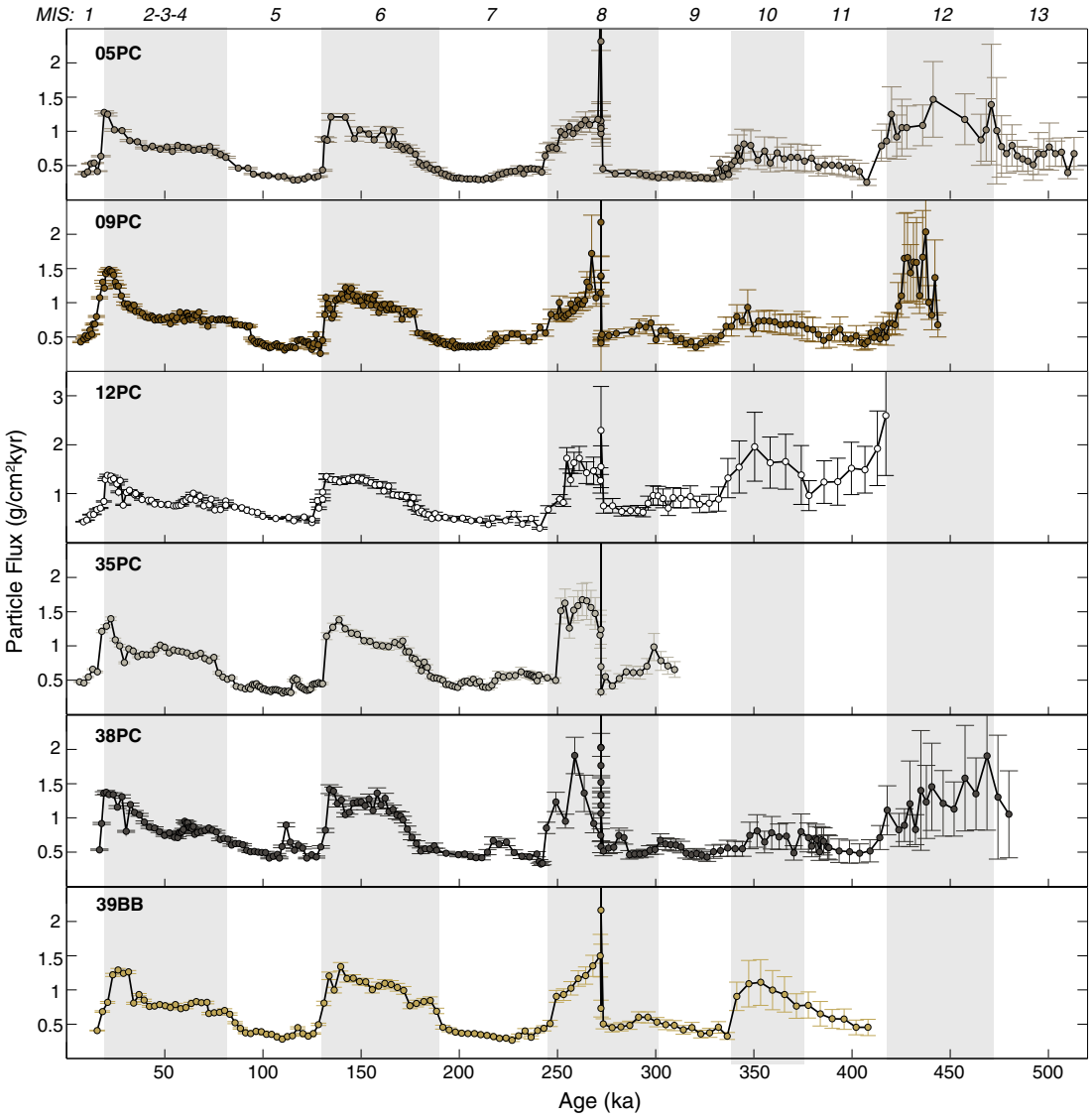

Fig. 3. ^{230}Th-based particle fluxes. Particle fluxes are higher during glacial MIS (gray bars) than during interglacial MIS by about a factor of two. High particle fluxes at 272 ka are associated with a magnetic susceptibility peak (Costa et al., 2016). Error bars indicate 2σ, which grows with the age of the sample.

Most cores contain periods of winnowing and periods of focusing, with focusing factors ranging from 0.16 to 3.43 (Fig. 4). Over the entire deposition period, the two cores (05PC and 39BB) farthest from the ridge are in near equilibrium with overlying water column ($\Psi = 1.04$–1.08), while 38PC and 12PC have net winnowing ($\Psi = 0.48$–0.73) and 35PC and 09PC have net focusing ($\Psi = 1.42$–1.73). Overall the region is net neutral, with $\Psi = 1.08$. While the other five cores fluctuated between the two modes, core 12PC experienced persistent winnowing ($\Psi = 0.16$–0.98), suggesting a relatively erosive environment as suspected from its lower than average total sedimentation rates (Costa et al., 2016). Near the coretops, 09PC and 35PC show particularly high focusing factors ($\Psi = 2.91$–3.43) corresponding to high total sedimentation rates (3.02–3.26 cm/kyr). There is no clear glacial-interglacial cycling in focusing factors, and instead they follow the disparate trends of total sedimentation rates.

4. DISCUSSION

4.1. Particle fluxes and rain rates on the Juan de Fuca Ridge

The glacial-interglacial cycling of particle flux mirrors the observed cycles in density and carbonate (Supplemental Fig. 1) that reflect carbonate preservation cycles in the Pacific Ocean (Farrell and Prell, 1989). Particle fluxes are high when density and $CaCO_3$ concentrations are also high. Independent of sediment focusing, the particle rain rates would scale with how much of the carbonate is preserved on the seafloor. If $CaCO_3$ is assumed to be zero during interglacial periods, then the interglacial particle flux

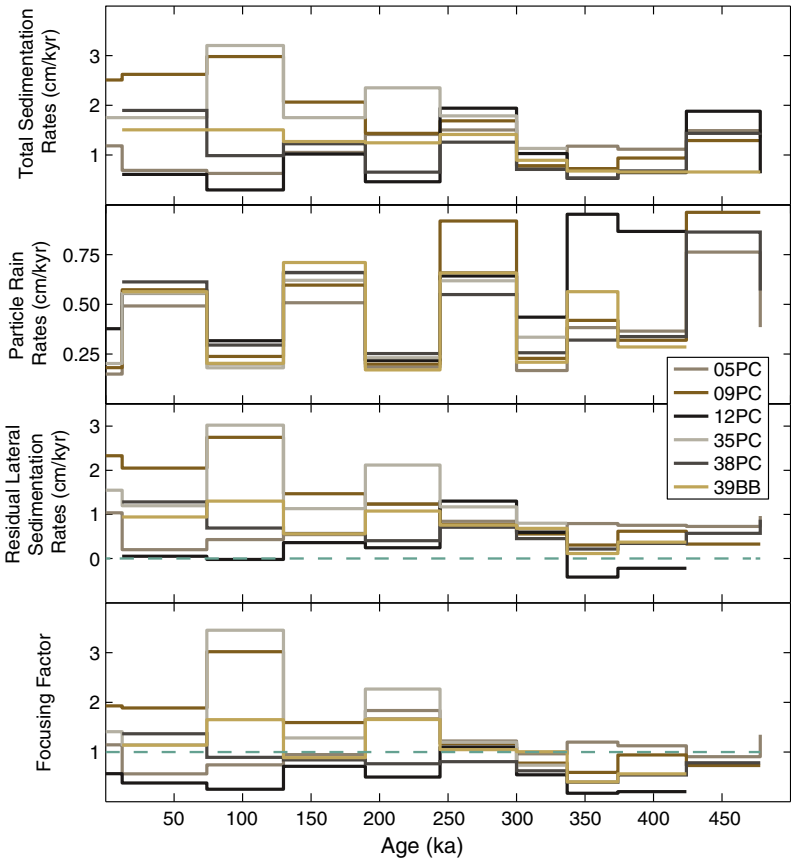

Fig. 4. Comparison of total sedimentation rates, particle rain rates, residual lateral sedimentation rates, and focusing factors. Total sedimentation, lateral sedimentation, and focusing factors all resemble one another, with high variability in each MIS, especially during the last 250 ka. Particle rain rates are almost always different from total sedimentation rates, and they are the only parameter to show clear and consistent glacial-interglacial cycles.

(0.53 g/cm^2 kyr) can be modeled as the noncarbonate flux, which appears relatively constant over time. Then the preservation of glacial carbonate rain would contribute 0.45 g/cm^2 kyr of carbonate, accounting for the near doubling of particle flux. These rudimentary estimates would predict glacial $CaCO_3$ concentrations of nearly 50 wt%, which would not be inconsistent with actual glacial values observed in these cores (50–70 wt%). Therefore it would be reasonable to attribute the glacial-interglacial pattern of particle flux variations almost entirely to changes in preserved carbonate flux.

The large temporal fluctuations in particle flux easily overshadow the concurrent spatial variability between cores. Over the more recent 300 kyr, particle flux varies between cores by $\leqslant$0.15 g/cm^2 kyr, or about 14–16% in glacial periods and 7–27% in interglacial periods (Fig. 5). These intercore differences are exceptionally low, considering the nearly order of magnitude differences between the cores in total sedimentation rates (Costa et al., 2016). Intercore variability increases in MIS8 (31%) and continues to grow through MIS9, 10, and 11 due primarily to the divergence of 12PC from the other five cores. Excluding 12PC, the intercore variability would be about the same >300 ka as it is <300 ka. Fluxes at 12PC are at times more than double what is observed at the other cores.

Elevated fluxes at 12PC may be related to distance from the ridge and the input of hydrothermal particles (Supplemental Fig. 2). Particle fluxes are likely to be higher closer to the ridge, as heavy plume fallout, particularly basalt glass and sulfide grains, are limited to within several kilometers of the vent site (e.g., Clague et al., 2009). The bottom of 12PC contains abundant basalt glass that suggests hydrothermal and magmatic activity that corresponds with the high fluxes associated with the interval when the core was within 10 km of the ridge. The decline in excess flux with increasing distance of the ridge would be consistent with decreasing hydrothermal inputs as 12PC became more distal, until >10 km when the additional particle flux reaches approximately zero, as observed in the other 5 cores. Alternatively, the high fluxes in 12PC may be a function of the extreme winnowing ($\Psi = 0.158$–0.205) taking place at that site at that time (Supplemental Fig. 2). Winnowing may bias particle flux reconstructions by preferentially removing Th-rich fine material, thus reducing the Th inventory and inflating particle fluxes (Marcantonio et al., 2014). In this case, the high fluxes at 12PC may indicate a threshold effect in winnowing: the bias towards high fluxes is clearly apparent when $\Psi = 0.158$–0.205 (12PC, MIS10, 11) but appears negligible when $\Psi = 0.243$ (12PC, MIS5) or higher. At this time it is difficult to conclusively

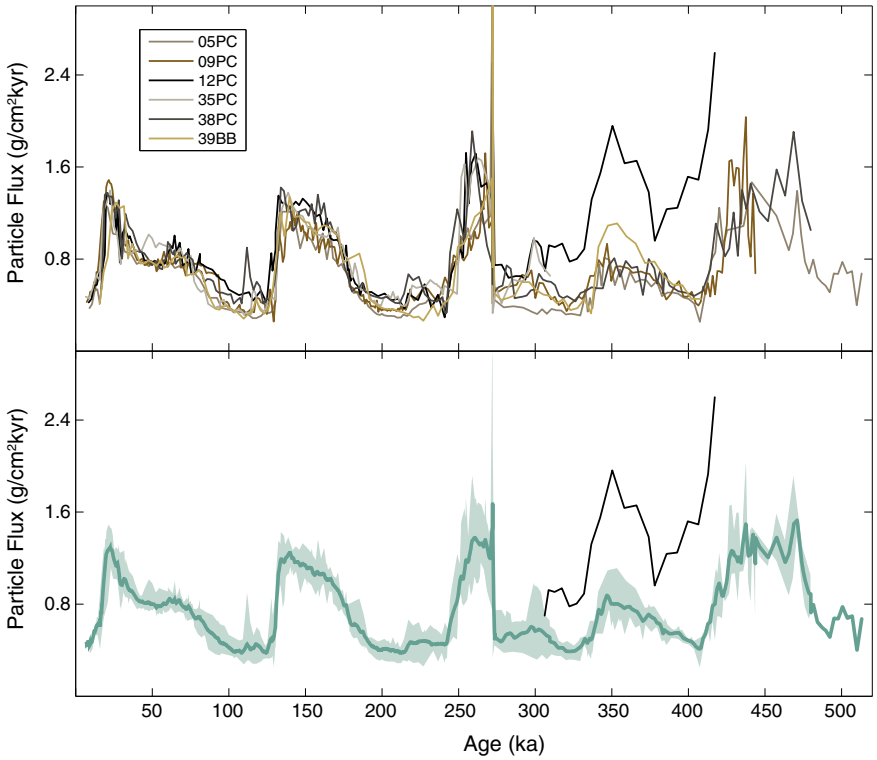

Fig. 5. Compiled particle flux. When overlain together, it is apparent that particle fluxes from the six different cores are nearly identical for the last 300 kyr. Older than 300 ka, 12PC diverges to higher particle fluxes than the other cores. *Bottom*: Average particle flux, with shading that indicates the full range of values at each time step. Note the small variability envelope for the last 300 ka. Older than 300 ka, 12PC is shown as a black line and it is not included in the shaded envelope showing the range of values.

interpret the high fluxes in 12PC in favor of hydrothermal activity or winnowing, but future work on hydrothermal deposition (e.g., Fe, Mn fluxes) may prove decisive.

Particle rain rates can be obtained by scaling the particle flux by the dry bulk density (g/cm^3) (see Methods Section 2.3) (Fig. 4). Because particle flux and dry bulk density are in phase, the scaling merely adjusts the amplitude of, or exaggerates the difference between, the glacial-interglacial cycles. Thus particle rain rates retain clear carbonate preservation cycles, with increased particle rain rates during glacial periods (0.55–1.06 cm/kyr) compared to interglacial periods (0.16–0.40 cm/kyr). Particle rain rates are comparable across all six cores, varying by as low as 4.8% during MIS2-3-4. Such consensus is not unexpected given the close proximity of the cores (<50 km) and the relatively homogeneous surface productivity at this spatial scale (e.g., Kienast et al., 2007).

Particle rain rates are much more consistent than total sedimentation rates, which show considerable variability between the core sites, as much as 500% difference (MIS5: 0.61 cm/kyr at 05PC vs 3.18 cm/kyr at 35PC; Costa et al., 2016). There is little to no correlation between total sedimentation rates and particle rain rates (Fig. 6), but variability in total sedimentation rates seems to increase as the particle rain rate decreases. While particle rain rates of >1 cm/kyr might co-occur with total sedimentation rates of 0.41–1.09 cm/kyr, particle rain rates of 0.4 cm/kyr could correspond with total sedimentation rates anywhere from 0.25 to 3.26 cm/kyr. The independent variability in total sedimentation rates and particle rain rates indicates that changes in the particle rain rate are not the dominant influence on total sedimentation on the JdFR. This discrepancy highlights the potential errors in interpretation that may be introduced when using age model based total sedimentation rates rather than particle rain rates based on constant flux proxies.

4.2. Focusing factors

Sedimentation rates are primarily controlled by two factors: the particle rain rate of pelagic sediment and the intensity of sediment redistribution along the seafloor (Hauschild et al., 2003). The lack of dependence of total sedimentation rates on particle rain rates suggests that sediment redistribution must be the dominant influence on the spatial variability in sediment deposition on the JdFR. Sediment redistribution can be parameterized using ^{230}Th systematics from two different perspectives: (1) residual lateral sedimentation and (2) focusing factors. Residual lateral sedimentation, as required by mass balance, can be calculated as the difference between total sedimentation rate and particle rain rate. Focusing factors are calculated based on the loss or gain of ^{230}Th above the production value (see Section 2.4), which is carried by ^{230}Th-laden sedimentary particles. Focusing factors and lateral sedimentation rates show the same pattern, so that both parameters are high

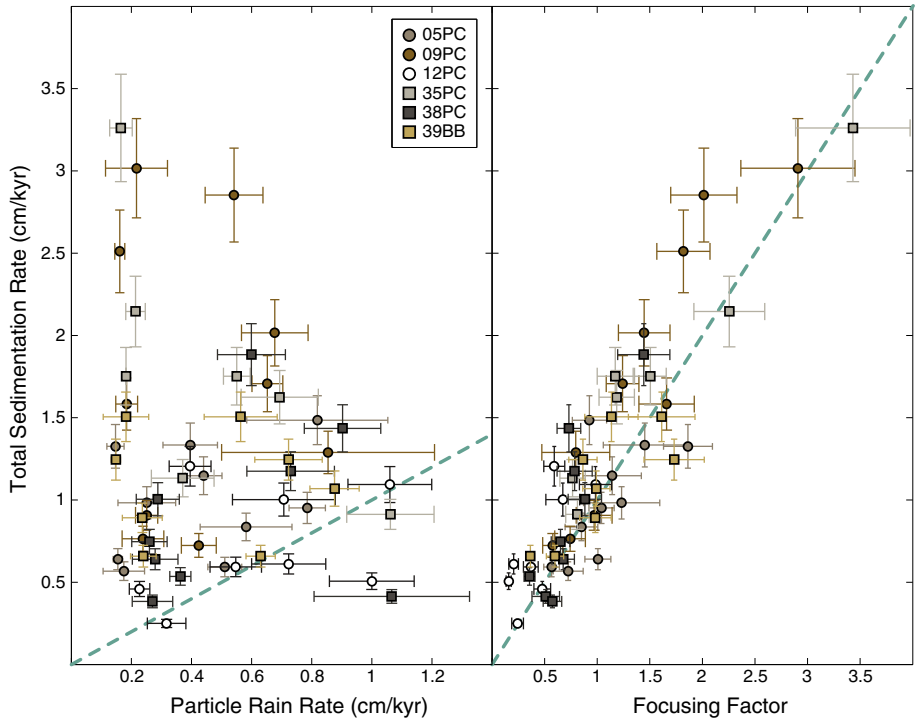

Fig. 6. Scatter plots comparing total sedimentation rates, particle rain rates, and focusing factors. Total sedimentation rate shows little to no relationship with particle rain rate, whereas it has a strong positive, linear correlation with focusing factors ($r^2 = 0.80$). Dashed teal lines are 1:1 lines.

when total sedimentation rates are high (Fig. 4), and especially when particle rain rates are simultaneously low (e.g., MIS5 and MIS7). The nearly one to one relationship between focusing factors and total sedimentation rates reflects variability in sediment redistribution on small spatial scales (Fig. 6), 10s of kilometers or less (Kienast et al., 2007). During MIS5, focusing at 35PC ($\Psi = 3.43$) and 12PC ($\Psi = 0.24$) is an order of magnitude different despite these sites being only 10.5 km apart. This is in direct contrast to previous conclusions that sediment redistribution occurs on large spatial and temporal scales (Lyle et al., 2005). Sediment focusing is instead highly variable over small distances, and focusing, rather than particle flux, is the most important mechanism for total sedimentation on the JdFR and potentially in other topographically rugged regions.

Even though focusing is highly variable and strongly controls total sedimentation, it does not interfere with the utility of ^{230}Th to reconstruct particle rain rate on the JdFR. It has long been recognized that ^{230}Th is concentrated in the fine fraction due to the high surface area to volume ratio (Suman and Bacon, 1989; Francois et al., 1990, 2004; Thomson et al., 1993; McGee et al., 2010; Kretschmer et al., 2010). By extension, focusing (adding fine fraction) and winnowing (removing fine fraction) have been proposed to fractionate ^{230}Th and bias the particle rain rate reconstruction. Focused sites would contain excess ^{230}Th, thus underestimating the true particle rain rate, and winnowed sites would have a deficit of ^{230}Th, thus overestimating the particle rain rate (Marcantonio et al., 2014). But on the JdFR, with the possible exception of >300 ka in 12PC (see Section 4.1), there is no dependence of the particle rain rate on the focusing factor (Fig. 7). In MIS5, for example, the focusing factor has a wide range from 0.24 to 3.43, whereas the particle flux is narrowly constrained to 0.22 ± 0.06 g/cm^2 kyr. The variability between cores is nearly equivalent to the variability within a single core during the same time period (e.g., 0.22 ± 0.10 g/cm^2 kyr in 09PC during MIS5). This general lack of correlation between focusing factors and particle flux reconstruction demonstrates that decoupling of ^{230}Th from the sediment mass during sediment redistribution is negligible and does not interfere with the ^{230}Th systematics.

Sediment focusing is typically associated with fine fraction, so that more focused sites are expected to skew towards finer grain size distributions (e.g., lower coarse fractions) (Lyle et al., 2005, 2014; Kretschmer et al., 2010; Marcantonio et al., 2014). On the JdFR, the two highest incidents of focusing ($\Psi = \sim$3–3.5) coincide with low coarse fraction (<5%, Costa et al., 2016), but without those points any relationship between coarse fraction and focusing weakens (Fig. 8). Sediment focusing ($\Psi = 1.5$) can result in sediment with 2%, 20%, or 35% coarse fraction, but sediment winnowing ($\Psi = 0.75$) could just as well generate those size distributions. Thus, while the fine fraction may be more susceptible to sediment redistribution, its preferential mobility along the seafloor does not significantly affect the ^{230}Th systematics.

The resilience of ^{230}Th to focusing may be derived from two different aspects of sediment redistribution. First, most

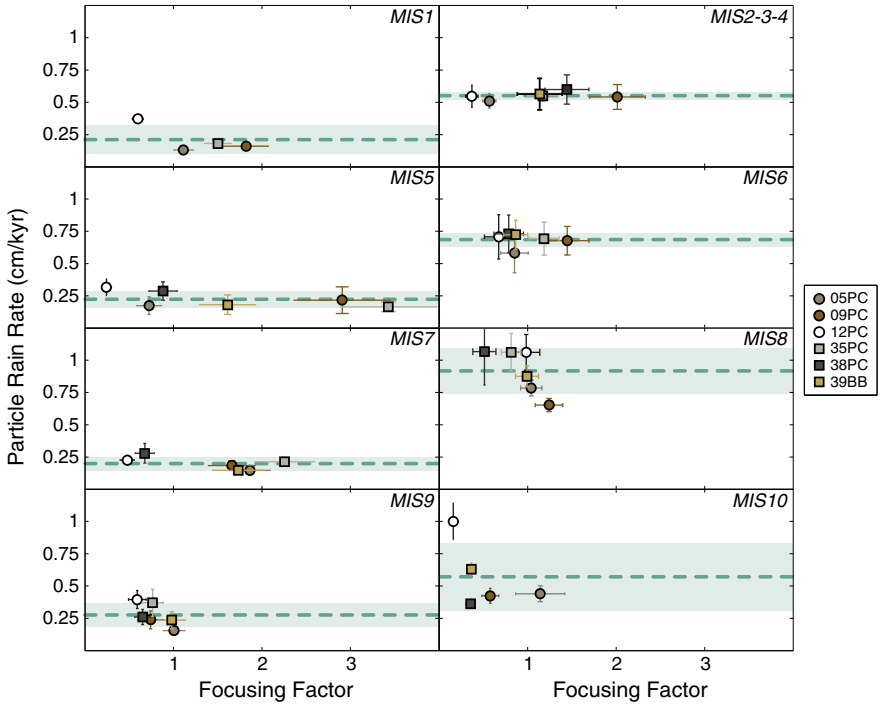

Fig. 7. Particle rain rates and focusing factors during each MIS. Particle rain rates are nearly constant regardless of the focusing factors, indicating no biases in ^{230}Th normalization due to sediment redistribution. Dashed teal lines are the MIS averages, and shaded regions are the 1σ range. Cores 38PC and 39BB do not extend into MIS1; their coretop ages are in late MIS2. Variability in MIS8 is largely due to high particle fluxes associated with the magnetic susceptibility peak at 272 ka.

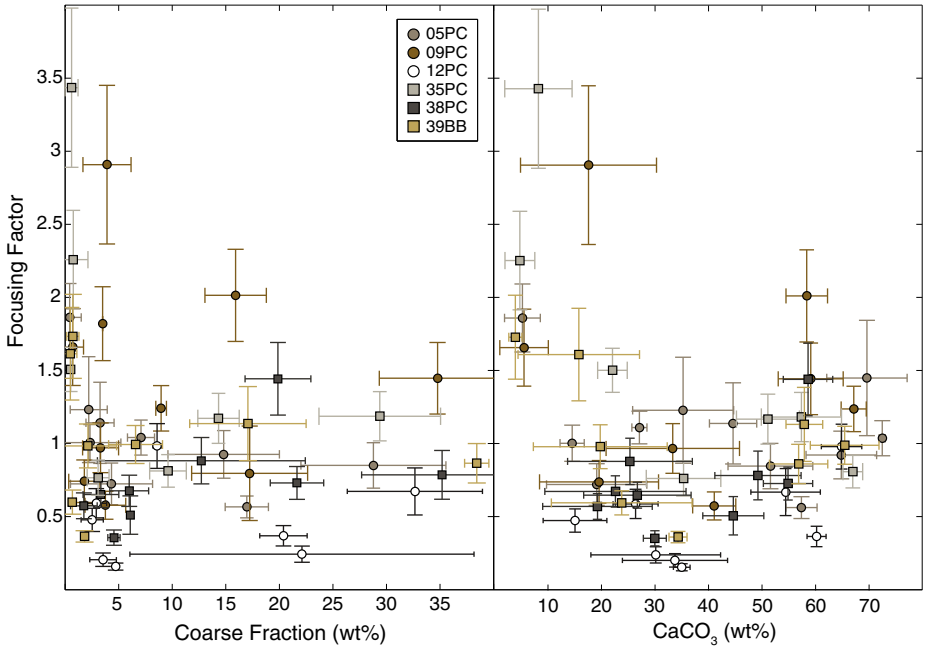

Fig. 8. Focusing factors, coarse fraction, and carbonate content. Each datapoint represents are the MIS average, and the error bars are 1σ. The highest focusing factors coincide with low coarse fraction and low calcium carbonate, but otherwise no strong relationship is observed between focusing factor and these two parameters. Carbonate concentrations may have a parabolic relationship with focusing factor, but the Juan de Fuca Ridge does not achieve high enough carbonate contents (>80 wt%) to fully assess this observation.

pelagic sediment is relatively fine (<35% coarse), so that the size distributions between particle rain rate and lateral sedimentation may not be incongruous (McGee et al., 2010). For example, 50% winnowing ($\Psi = 0.5$) of sediment that

starts as 5 wt% coarse will only increase the coarse fraction to 8.3 wt%. Similarly, 50% focusing ($\Psi = 1.5$) of purely fine material to that 5 wt% coarse sediment would only decrease the coarse fraction to 3.7 wt%. Such small changes in the coarse fraction are comparable to the variability in coarse fraction within a MIS period, and they suggest that the grain size distribution may not be particularly sensitive to the lateral flux of sediments. Second, the cohesion of fine particles may inhibit their resuspension from the seafloor and increase their effective particle size (McCave and Hall, 2006; McGee et al., 2010). Small ^{230}Th-rich particles (2 μm, Kretschmer et al., 2010) are likely to aggregate into much larger particles (10 μm) that would be significantly less mobile (McCave and Hall, 2006; McGee et al., 2010). This relatively small change in grain size appears to be effective in mitigating ^{230}Th fractionation even at relatively low current speeds, such as the zero-mean oscillatory currents (sporadically up to 10 cm/s) observed on the JdFR (Thomson et al., 2003). Alternatively, the effects of grain size may only become relevant under extreme endmember conditions, such as the much higher coarse fractions (>35 wt%) that can be observed in the Equatorial Pacific.

Similarly, the influence of carbonate content on ^{230}Th systematics may only be important in extremely carbonate rich sediments (>80 wt%), especially when much of this carbonate is in the coarse fraction (Marcantonio et al., 2014). The highest focusing factors on the JdFR are associated with low (but not the lowest) carbonate content, but otherwise there is little relationship between focusing and carbonate composition (Fig. 8). Winnowing can result in a core with 20% $CaCO_3$ or 60% $CaCO_3$, just as well as focusing can do the same. This observation argues against a bias towards underestimating ^{230}Th in carbonate rich sediments, most likely due to the relatively uniform distribution of ^{230}Th on coarse and fine carbonate material in contrast to the fine skew in siliceous sediments (Kretschmer et al., 2010). Because there is no evident relationship between carbonate and focusing, we can be confident in the continued utility of ^{230}Th normalization in carbonate-variable sediments.

5. CONCLUSIONS

On the Juan de Fuca Ridge, ^{230}Th normalization from six different cores produces a robust record of particle rain rate over the last 510 kyr. Particle rain rates are high during glacial periods and low during interglacial periods, following the carbonate preservation cycles in the Pacific. Particle rain rates frequently differ from age-model based total sedimentation rates, which are largely controlled by sediment focusing. Despite previous conjectures, no relationships have been found amongst focusing factors, grain size, and carbonate content that would suggest any disturbance in ^{230}Th systematics by sediment focusing and/or dissolution. Therefore, given the lack of correspondence between age-model versus ^{230}Th-normalized sedimentation rates, this study demonstrates the importance of using constant flux proxies when reconstructing particle rain rates.

Furthermore, this study provides the unique opportunity to determine the fate and transport of sediment on the seafloor in a relatively closed sedimentary system. Because the cores are so close together (<50 km), the particle rain rate is both expected and demonstrated to be spatially homogeneous. In contrast, sediment redistribution is highly variable in the study area, with an order of magnitude range in focusing factors. Yet while some cores display net focusing (09PC, 35PC) and others display net winnowing (12PC, 38PC), the region as a whole is net neutral, with no large-scale import or export of sediment. This targeted demonstration exemplifies the processes that must, by necessity, apply to sedimentation on the sea floor globally. Thus the validation of ^{230}Th normalization on the Juan de Fuca Ridge presented here is likely to be an expression of its extensive efficacy in the world ocean.

ACKNOWLEDGEMENTS

The authors thank Martin Fleisher for technical assistance with U-Th chemistry and Kelly Luis for assistance with carbonate analyses. Robert Anderson and Gisela Winckler provided insightful discussion that helped improve this manuscript. We thank Franco Marcantonio and one anonymous reviewer for their valuable feedback in their reviews. This research was funded by NSF-FESD-#1338832 to J.F.M. and a National Science Foundation Graduate Research Fellowship to K.M.C.

APPENDIX A. SUPPLEMENTARY DATA

Supplementary data associated with this article can be found, in the online version, at http://dx.doi.org/10.1016/j.gca.2016.10.034.

REFERENCES

Anderson R. F., Bacon M. P. and Brewer P. G. (1983) Removal of ^{230}Th and ^{231}Pa at ocean margins. *Earth Planet. Sci. Lett.* **66**, 73–90.

Anderson R. F., Fleisher M. Q., Lao Y. and Winckler G. (2008) Modern CaCO3 preservation in equatorial Pacific sediments in the context of late-Pleistocene glacial cycles. *Mar. Chem.* **111**, 30–46.

Bacon M. P. (1984) Glacial to interglacial changes in carbonate and clay sedimentation in the Atlantic Ocean estimated from 230Th measurements. *Isot. Geosci.* **2**, 97–111.

Broecker W. (2008) Excess sediment 230 Th: Transport along the sea floor or enhanced water column scavenging? *Global Biogeochem. Cycles* **22**.

Broecker W. S. (1971) Calcite accumulation rates and glacial to interglacial changes in oceanic mixing. In *The Late Cenozoic Glacial Ages* (ed. K. K. Turekian). Yale University Press, New Haven, CT, pp. 239–265.

Cheng H., Lawrence Edwards R., Shen C. C., Polyak V. J., Asmerom Y., Woodhead J., Hellstrom J., Wang Y., Kong X., Spötl C., Wang X. and Calvin Alexander E. (2013) Improvements in 230Th dating, 230Th and 234U half-life values, and U-Th isotopic measurements by multi-collector inductively coupled plasma mass spectrometry. *Earth Planet. Sci. Lett.* **371–372**, 82–91.

Clague D. A., Paduan J. B. and Davis A. S. (2009) Widespread strombolian eruptions of mid-ocean ridge basalt. *J. Volcanol. Geotherm. Res.* **180**, 171–188.

Costa K. M., McManus J. F., Boulahanis B., Carbotte S. M., Winckler G., Huybers P. and Langmuir C. H. (2016) Sedimentation, stratigraphy and physical properties of sediment on the Juan de Fuca Ridge. *Mar. Geol.* **380**, 163–173.

Farrell J. W. and Prell W. L. (1989) Climatic change and CaCO3 Preservation: An 800,000 year bathymetric reconstruction from the Central Equatorial Pacific Ocean. *Paleoceanography* **4**, 447–466.

Fleisher M. Q. and Anderson R. F. (2003) Assessing the collection efficiency of Ross Sea sediment traps using 230Th and 231Pa. *Deep Sea Res. Part II Top. Stud. Oceanogr.* **50**, 693–712.

Francois R., Bacon M. P. and Suman D. O. (1990) Thorium230 profiling in deep-sea sediments: High resolution records of flux and dissolution of carbonate in the Equatorial Atlantic during the last 24,000 years. *Paleoceanography* **5**, 761–787.

Francois R., Frank M., Rutgers van der Loeff M. and Bacon M. P. (2004) ^{230}Th normalization: an essential tool for interpreting sedimentary fluxes during the late Quaternary. *Paleoceanography* **19**, PA1018.

Francois R., Frank M., Rutgers van der Loeff M., Bacon M. P., Geibert W., Kienast S., Anderson R. F., Bradtmiller L., Chase Z., Henderson G., Marcantonio F. and Allen S. E. (2007) Comment on "Do geochemical estimates of sediment focusing pass the sediment test in the equatorial Pacific?" by M. Lyle et al.. *Paleoceanography* **22**, PA1216.

Hauschild J., Grevemeyer I., Kaul N. and Villinger H. (2003) Asymmetric sedimentation on young ocean floor at the East Pacific Rise, 15 S. *Mar. Geol.* **193**, 49–59.

Henderson G. M. and Anderson R. F. (2003) The U-series Toolbox for Paleoceanography. *Rev. Mineral. Geochemistry* **52**, 493–531.

Henderson G. M., Heinze C., Anderson R. F. and Winguth A. M. E. (1999) Global distribution of the 230Th flux to ocean sediments constrained by GCM modelling. *Deep Sea Res. I* **46**, 1861–1893.

Johnson D. A. and Johnson T. C. (1970) Sediment redistribution by bottom currents in the central Pacific. *Deep Sea Res.* **17**, 157–169.

Keigwin L. D. and Schlegel M. A. (2002) Ocean ventilation and sedimentation since the glacial maximum at 3 km in the western North Atlantic. *Geochem. Geophys. Geosyst.* **3**.

Kienast S. S., Kienast M., Mix A. C., Calvert S. E. and François R. (2007) Thorium-230 normalized particle flux and sediment focusing in the Panama Basin region during the last 30,000 years. *Paleoceanography* **22**.

Kretschmer S., Geibert W., Rutgers van der Loeff M. M. and Mollenhauer G. (2010) Grain size effects on 230Thxs inventories in opal-rich and carbonate-rich marine sediments. *Earth Planet. Sci. Lett.* **294**, 131–142.

Loubere P., Mekik F., Francois R. and Pichat S. (2004) Export fluxes of calcite in the eastern equatorial Pacific from the Last Glacial Maximum to present. *Paleoceanography* **19**, PA2018.

Lyle M., Mitchell N., Pisias N., Mix A., Martinez J. I. and Paytan A. (2005) Do geochemical estimates of sediment focusing pass the sediment test in the equatorial Pacific? *Paleoceanography* **20**.

Lyle M., Pisias N., Paytan A., Martinez J. I. and Mix A. (2007) Reply to comment by R. Francois et al. on "Do geochemical estimates of sediment focusing pass the sediment test in the equatorial Pacific?": Further explorations of ^{230}Th normalization. *Paleoceanography* **22**.

Lyle M., Marcantonio F., Moore W. S., Murray R. W., Huh C., Finney B. P., Murray D. W. and Mix A. C. (2014) Sediment size fractionation and focusing in the equatorial Pacific: effect on 230Th normalization and paleo flux measurements. *Paleoceanography* **29**, 747–763.

Marcantonio F., Lyle M. and Ibrahim R. (2014) Particle sorting during sediment redistribution processes and the effect on 230Th-normalized mass accumulation rates. *Geophys. Res. Lett.* **41**, 5547–5554.

McCave I. N. and Hall I. R. (2006) Size sorting in marine muds: processes, pitfalls, and prospects for paleoflow-speed proxies. *Geochem. Geophys. Geosyst.* **7**.

McGee D., Marcantonio F., McManus J. F. and Winckler G. (2010) The response of excess 230Th and extraterrestrial 3He to sediment redistribution at the Blake Ridge, western North Atlantic. *Earth Planet. Sci. Lett.* **299**, 138–149.

McManus J. F., Anderson R. F., Broecker W. S., Fleisher M. Q. and Higgins S. M. (1998) Radiometrically determined sedimentary fluxes in the sub-polar North Atlantic during the last 140,000 years. *Earth Planet. Sci. Lett.* **155**, 29–43.

Mitchell N. C. and Huthnance J. M. (2013) Geomorphological and geochemical evidence (230Th anomalies) for cross-equatorial currents in the central Pacific. *Deep Sea Res. Part I Oceanogr. Res. Pap.* **78**, 24–41.

Nozaki Y., Horibe Y. and Tsubota H. (1981) The water column distributions of thorium isotopes in the western North Pacific. *Earth Planet. Sci. Lett.* **54**, 203–216.

Owens S. A., Buesseler K. O. and Sims K. W. W. (2011) Re-evaluating the 238U-salinity relationship in seawater: Implications for the 238U–234Th disequilibrium method. *Mar. Chem.* **127**, 31–39.

Ruhlemann C., Frank M., Hale W., Mangini A., Mulitza S., Muller P. J. and Wefer G. (1996) Late Quaternary productivity changes in the western equatorial Atlantic: Evidence from Th-230-normalized carbonate and organic carbon accumulation rates. *Mar. Geol.* **135**, 127–152.

Singh A. K., Marcantonio F. and Lyle M. (2013) Water column 230Th systematics in the eastern equatorial Pacific Ocean and implications for sediment focusing. *Earth Planet. Sci. Lett.* **362**, 294–304.

Suman D. O. and Bacon M. P. (1989) Variations in Holocene sedimentation in the North American Basin determined from 230Th measurements. *Deep Sea Res.* **36**, 869–878.

Taylor S. R. and McLennan S. M. (1995) The geochemical evolution of the continental crust. *Rev. Geophys.*, 241–265.

Thomson J., Colley S., Anderson R. F., Cook G. T., MacKenzie A. B. and Harkness D. D. (1993) Holocene sediment fluxes in the Northeast Atlantic from 230Thexcess and radiocarbon measurements. *Paleoceanography* **8**, 631–650.

Thomson R. E., Mihaly S. F., Rabinovich A. B., McDuff R. E., Veirs S. R. and Stahr F. R. (2003) Constrained circulation at Endeavour ridge facilitates colonization by vent larvae. *Nature* **424**, 545–549.

Associate editor: Timothy J. Shaw